A Real-Time Attack Localization Algorithm for Large Power System Networks Using Graph-Theoretic Techniques

Thomas R. Nudell, *Student Member, IEEE*, Seyedbehzad Nabavi, *Student Member, IEEE*, and Aranya Chakrabortty, *Senior Member, IEEE*

***Abstract*—We develop a graph-theoretic algorithm for localizing the physical manifestation of attacks or disturbances in large power system networks using real-time synchrophasor measurements. We assume the attack enters through the electromechanical swing dynamics of the synchronous generators in the grid as an unknown additive disturbance. Considering the grid to be divided into coherent areas, we pose the problem as to localize which area the attack may have entered using relevant information extracted from the phasor measurement data. Our approach to solve this problem consists of three main steps. We first run a phasor-based model reduction algorithm by which a dynamic equivalent of the clustered network can be identified in real-time. Second, in parallel, we run a system identification in each area to identify a transfer matrix model for the full-order power system. Thereafter, we exploit the underlying graph-theoretic properties of the identified reduced-order topology, create a set of localization keys, and compare these keys with a selected set of transfer function residues. We validate our results using a detailed case study of the two-area Kundur model and the IEEE 39-bus power system.**

***Index Terms*—Algebraic graph theory, attack localization, identification, nodal domains, power system.**

I. Introduction

OVER THE past decade, the North American power system industry has witnessed a massive transformation in monitoring and control paradigms. This overhaul includes the deployment of wide-area measurement systems consisting of hundreds of new phasor measurement units (PMUs), which are capable of streaming geo-synchronized dynamic measurements via Ethernet connections in near real-time, effectively creating the backbone of a cyber layer on top of the physical model of the power grid [1]. In the current state-of-the-art, PMU data are primarily used for offline postmortem analysis of disturbance events including oscillation monitoring [2], voltage stability monitoring, and phasor-based state estimation [3], [4], in addition to recent developments in closed-loop control [5]. However, a very limited amount of research has evaluated how synchrophasors, beyond analyzing offline disturbance events, can also be used for online detection, and, more importantly, localization of faults and malicious attacks. Several recent papers have studied how false-data injection attacks may be deceptively injected into a power grid via its state estimation loops [6]–[9], while others have proposed estimation-based mitigation strategies to secure the grid against some of these attacks [10], [11]. However, the problem of localizing an attack in a large grid—in real-time as the grid dynamics are evolving—remains a widely open challenge. This problem, in fact, is becoming ever more important as the conventional grid continues to be integrated with new renewable energy sources and new loads such as electric vehicle and smart buildings, each of which contribute its own share of complexity and uncertainty to the grid dynamics. For example, a malfunctioning valve, due to natural or malicious failure, at a power plant cycling full-on and full-off may excite the electromechanical swing dynamics of the generators as reported in [12]. System operators are, therefore, constantly looking for fast numerical techniques by which PMU data spread across various parts of the grid can be efficiently processed to localize disturbances.

Motivated by this problem, in this paper, we propose a multistage localization algorithm based on the graph-theoretic properties of the physical topology of the power system network. Disturbances, caused by natural faults or malicious attacks, can enter the grid operation as denial-of-service attacks, flooding or jamming of communication links, corruption of feedback signals [13], spoofing of global positioning system (GPS) synchronization [14], and so on. For convenience of analysis, we will assume that no matter the source of the anomaly, the fault or attack effectively enters the dynamics of the power system as an unknown additive disturbance signal through the electro-mechanical swing equations of its generators. In other words, our basic assumption is that the impact of the incoming disturbance manifests itself as an exogenous input to the power balance dictating its swing dynamics. Our goal is to gather PMU data from multiple locations and extract information from these data to determine the location of the node where this disturbance signal may have been injected. However, in this context, the sheer size and complexity of the grid may make localization at that level of granularity practically intractable in real-time. Therefore, we relax our

Manuscript received May 16, 2014; revised September 22, 2014; accepted December 29, 2014. Date of publication March 10, 2015; date of current version August 19, 2015. This work was supported in part by the National Science Foundation, Division of Electrical, Communications, and Cyber Systems under Grant 1062811. Paper no. TSG-00462-2014.

The authors are with the Department of Electrical and Computer Engineering, North Carolina State University, Raleigh, NC 27606 USA (e-mail: trnudell@ncsu.edu; snabavi@ncsu.edu; achakra2@ncsu.edu).

Color versions of one or more of the figures in this paper are available online at http://ieeexplore.ieee.org.

Digital Object Identifier 10.1109/TSG.2015.2406571

formulation by assuming the transmission network is divided into a finite number of coherent clusters, and pose the problem as to develop a PMU-based real-time algorithm by which an operator can quickly localize the *cluster* in which the disturbance may have occurred.

Our proposed algorithm utilizes theoretical results reported recently in [15]. However, the algorithms in [15] requires offline *a priori* analysis as well as several nonidealistic assumptions about the network topology. In contrast, in this paper, we develop a completely real-time algorithm by dividing the localization problem into two parts. First, we utilize PMU data transmitted from the different clusters, or utility companies, to the control center of an independent system operator (ISO), and run a model reduction algorithm by which a dynamic equivalent of the clustered network is identified in real-time [16]. Second, in parallel to the model reduction step, we run a system identification routine in every cluster using local PMU data to identify a transfer matrix model for the full-order power system. Once the model reduction step is completed, the ISO makes use of the underlying graph-theoretic properties of the identified reduced-order topology, creates a set of localization keys, and transmits the relevant back to each local cluster keys via a wide-area communication network. Once the local clusters complete their individual system identification steps, and receive the keys from the ISO, each independently compares a selected set of residues in their identified transfer matrices with those keys, and thereby infers the identity of the cluster where the disturbance may have entered using graph-theoretic properties of the full-order network. A notable advantage of this algorithm is that it is completely measurement-based, and therefore, requires minimal knowledge about the actual model of the grid. Moreover, it requires communication of PMU data only between the utilities and the ISO, not between the utilities themselves, and thereby maintains data privacy. Our results are theoretically more rigorous than [17], and at the same time numerically more tractable than traditional localization methods as in [11] and [18]. We illustrate our algorithm with a detailed case study of the two-area Kundur system, then summarize results of an attack on the IEEE 39-bus power system network.

The remaining sections are organized as follows. Section II introduces the notation used throughout this paper and provides the requisite graph-theoretic definitions. Section III formulates the disturbance localization problem and provides an overview of the solution strategy in three distinct steps. Section IV details each of the three steps of our localization procedure. Section V provides a detailed cases study of the localization algorithm on the two area Kundur model, followed by an illustrative demonstration with the IEEE 39-bus system. Section VI concludes this paper.

II. Notation

This section briefly introduces the notation and provides important graph-theoretic definitions that will be referred to throughout this paper. For the real or complex scalar a, we let $|a|$ denote its modulus, and for the set $\mathcal{S}$, we let $|\mathcal{S}|$ denote its cardinality. For the matrix A or the vector x, we let $\|A\|$ or $\|x\|$ denote its norm (which will be clear from context), and let $[A]_{ij}$ or $[x]_i$ denote the (i,j)th element or ith component, respectively. We may also define a matrix with A_{ij} elements by $[A_{ij}]$, and define a $n \times n$ diagonal matrix by $\text{diag}[x_1, \ldots, x_n]$. The eigenvalues of a matrix $A \in \mathbb{R}^{n\times n}$ are denoted $\lambda(A) = \{\lambda_1, \ldots, \lambda_n\}$, where, by convention, we take $|\lambda_1| \leq |\lambda_2| \leq \cdots \leq |\lambda_n|$. We let v_k and w_k denote the right and left eigenvectors of A corresponding to eigenvalue λ_k. We let $I_{n\times n} \in \mathbb{R}^{n\times n}$, $0_{n\times m} \in \mathbb{R}^{n\times m}$, and $\mathbf{1}_n \in \mathbb{R}^n$ denote the identity matrix, zeros matrix, and vector of all ones, respectively. We let $e_l \in \mathbb{R}^n$ denote the unit indicator vector, where $[e_l]_k = 1$ when $k = l$ and $[e_l]_k = 0$ otherwise.

A. Graph Theory

A graph $\mathcal{G} = (\mathcal{V}, \mathcal{E})$ is a collection of vertices (or nodes) $\mathcal{V} = \{1, \ldots, n\}$ and edges $\mathcal{E} \subseteq \mathcal{V} \times \mathcal{V}$. The number of vertices in $\mathcal{G}$ is denoted $|\mathcal{V}| = n$. If there exists edge $kl \in \mathcal{E}$ then, we say the nodes $k,\ l \in \mathcal{V}$ are adjacent, and write $k \sim l$. The set of nodes adjacent to $l \in \mathcal{V}$ is called the neighborhood of l and denoted $\mathcal{N}_l = \{k \in \mathcal{V} |\ k \sim l\}$. We assume $\mathcal{G}$ is undirected, i.e., $l \sim k \Leftrightarrow k \sim l$, and that there are no loops or multiple edges between nodes. We assume every node $k \in \mathcal{V}$ has a real-valued weight $m_k > 0$, and every edge $kl \in \mathcal{E}$ has a real-valued weight $a_{kl} = a_{lk} > 0$. In a power system model, the node weight corresponds to the generator inertia constant, and the edge-weight is proportional to tie-line admittance. The symmetric, positive semidefinite graph Laplacian matrix associated with $\mathcal{G}$ is defined as $[L_\mathcal{G}]_{kl} = -a_{kl}$ when $k \sim l$, $[L_\mathcal{G}]_{kl} = \sum_{i\in\mathcal{N}_k} a_{ki}$ when $k = l$, and $[L_\mathcal{G}]_{kl} = 0$ otherwise. Unless specifically noted, we assume $\mathcal{G}$ is connected, thus the eigenvalues of $L_\mathcal{G}$ are ordered as $0 = \lambda_1 < \lambda_2 \leq \cdots \leq \lambda_n$. When there is no ambiguity we will drop the explicit reference to $\mathcal{G}$ and simply write L. We also define the asymmetric Laplacian matrix $L_m \triangleq M^{-1}L$, where $M = \text{diag}[m_1, \ldots, m_n] \in \mathbb{R}^{n\times n}$ is the node-weight matrix. Clearly L_m is also positive semidefinite.

We will use the following definition of weak discrete nodal domains, which we will simply refer to as nodal domains.

Definition 1: (Weak) Discrete Nodal Domain [19]: A positive (negative) nodal domain $\mathcal{D}$ of a real-valued vector $x \in \mathbb{R}^n$ is a maximal connected subgraph of $\mathcal{G}$ on nodes $k \in \mathcal{V}$ such that $[x]_k \geq 0$ ($[x]_k \leq 0$), where $|\mathcal{V}| = n$.

Throughout this paper, we will refer to the nodal domains of v_i, likewise w_i, as the λ_i nodal domains, where λ_i is an eigenvalue of $L_\mathcal{G}$ and v_i and w_i are corresponding right and left eigenvectors. Finally, from Definition 1, the following definition of adjacent nodal domains is immediate.

Definition 2: Two λ_i nodal domains $\mathcal{D}_1$ and $\mathcal{D}_2$ are adjacent if there exist vertices $k \in \mathcal{D}_1$ and $l \in \mathcal{D}_2 \setminus \mathcal{D}_1$ such that the edge $kl \in \mathcal{E}$.

III. Problem Formulation

Consider a n-bus power system network consisting of n^g synchronous generators and $n - n^g$ load buses. Without loss of generality, let $\{1, \ldots, n^g\}$ denote the generator buses. Let P_i and Q_i denote the total active and reactive power injected

into the ith bus, where

$$P_i = \sum_{k=1}^{n} -V_i^2 r_{ik}/z_{ik}^2 - V_i V_k \sin(\theta_{ik} - \alpha_{ik})/z_{ik} \quad (1a)$$

$$Q_i = \sum_{k=1}^{n} -V_i^2 x_{ik}/z_{ik}^2 + V_i V_k \cos(\theta_{ik} - \alpha_{ik})/z_{ik} \quad (1b)$$

where $V_i \angle \theta_i$ is the voltage phasor at the ith bus, $\theta_{ik} = \theta_i - \theta_k$, r_{ik} and x_{ik} are the resistance and reactance of the tie-line joining bus i with bus k, $z_{ik} = \sqrt{r_{ik}^2 + x_{ik}^2}$, and $\alpha_{ik} = \tan^{-1}(r_{ik}/x_{ik})$. For the rest of this paper, we will assume the line resistances to be equal to zero, since our objective is to localize disturbances in a reduced order model consisting of long tie-lines, for which neglecting line resistances is a reasonable assumption. The electromechanical model of the power system can be described as a system of differential-algebraic equations (DAEs) [20] as

$$\dot{\delta}_i(t) = \omega_s(\omega_i - 1) \quad (2a)$$

$$m_i \dot{\omega}_i(t) = P_i^m - P_i^e - d_i(\omega_i - 1) \quad (2b)$$

for $i = 1, \ldots, n^g$, and

$$0 = P_i^e + P_i - P_i^l, \quad 0 = Q_i^e + Q_i - Q_i^l \quad (3a)$$

$$0 = P_k - P_k^l, \quad 0 = Q_k - Q_k^l \quad (3b)$$

for $i = 1, \ldots, n^g$, and $k = n^g + 1, \ldots, n$. In (2), $\delta_i(t)$, $\omega_i(t)$, m_i, and d_i denote the internal rotor angle, speed, inertia, and damping of the ith generator, while P_i^m denotes the mechanical power input, P_i^e and Q_i^e denote the active and reactive electrical power produced by the ith generator. In (3), P_k^l and Q_k^l denote the active and reactive power consumed by the load at the kth bus. The DAE (2) can be converted into a system of purely differential equations via Kron reduction [21], resulting in a fully connected graph $\mathcal{G}^K$ with n^g nodes. Neglecting line losses and assuming P_i^m to be constant, its small-signal model linearized around $(\delta_0, \mathbf{1}_{n^g})$ following a disturbance in the network can be written as:

$$\begin{bmatrix} \Delta\dot{\delta} \\ \Delta\dot{\omega} \end{bmatrix} = \underbrace{\left[\begin{array}{c|c} 0_{n\times n} & \omega_s I_{n\times n} \\ \hline -L_m & -M^{-1}D \end{array}\right]}_{A} \begin{bmatrix} \Delta\delta \\ \Delta\omega \end{bmatrix} + \underbrace{\begin{bmatrix} 0 \\ \hline M^{-1}e_l \end{bmatrix}}_{B} u(t) \quad (4)$$

where $\Delta\delta = [\Delta\delta_1, \ldots, \Delta\delta_{n^g}]^T$, $\Delta\omega = [\Delta\omega_1, \ldots, \Delta\omega_{n^g}]^T$, $M = \mathrm{diag}[m_1, \ldots, m_{n^g}]$, $D = \mathrm{diag}[d_1, \ldots, d_{n^g}]$, and L_m is the asymmetric weighted Laplacian of the complete graph $\mathcal{G}^K$ with elements

$$[L_m]_{ki} = \begin{cases} -a_{ki}/m_k & \text{if } k \neq i \\ \sum_{\kappa \neq k} a_{k\kappa}/m_k & \text{if } k = i. \end{cases} \quad (5)$$

The edge weights of $\mathcal{G}^K$ are given as

$$a_{ki} = \frac{E_k E_i}{x_{ki}} \cos(\delta_{k0} - \delta_{i0}) \quad (6)$$

for all $k \neq i$, where voltage at the ith and kth generator E_i and E_k, respectively, are taken to be constant at this timescale. The vertex set of $\mathcal{G}^K$ is the set of generator buses $\mathcal{V} = \{1, \ldots, n^g\}$. For simplicity, we consider a single external disturbance $u(t) \in \mathbb{R}$ entering the network through acceleration equation of the lth generator, where the location l is unknown. Let $\mathcal{S} \subseteq \mathcal{V}$ denote a subset of $|\mathcal{S}| = h \leq n^g$ generator buses. We consider the output equations as

$$y(t) = C\Delta\delta(t) \quad (7)$$

where $y(t) = [y_1(t), \ldots, y_h(t)]^T$, and rows of C are of the form e_k^T, $k \in \mathcal{S}$. Ideally, we would like to identify the input location l directly, but as described in the introduction, achieving this in real-time for large power networks may be infeasible. Instead we assume the network to be divided into p coherent areas with disjoint sets of generators, denoted $\mathcal{V}^k$ with $k = 1, \ldots, p$, then, we take advantage of the resulting time-scale separation properties [22] of (6) to formulate our problem as: *following an attack on the network, rapidly localize the area(s) in which the attack input $u(t)$ may have entered using real-time synchrophasor measurements $y(t)$ from (7).*

To solve this problem, we propose the following three steps.

1) Assuming that each of the p coherent areas is represented by an equivalent generator connected over an equivalent topology $\mathcal{G}^E$, develop a real-time algorithm by which the equivalent topology $\mathcal{G}^E$ can be identified using $y(t)$.
2) Construct a set of localization keys—described in Section IV-B—based on the identified graph $\mathcal{G}^E$ which maps input-output locations in the network to the residues of the transfer function of the equivalent model.
3) Develop a real-time localization algorithm that utilizes the keys from Step 2) by the following.
   a) Estimate poles and residues of the transfer function of (4)–(7) via a system identification algorithm using $y(t)$.
   b) Exploit the relationship between the poles and residues of the reduced-order equivalent system explained in Section IV-B to build an estimated localization key.
   c) Compare the estimated localization key to the set of keys provided in Step 2) to localize the area(s) in which the input $u(t)$ may have entered.

The overall cyber-physical architecture for implementing these steps is shown in Fig. 1. In this figure, the power system is assumed to be divided into three coherent clusters, denoted as Areas 1, 2, and 3. Each area is equipped with a control center of its own, here represented simply by a phasor data concentrator (PDC). PMUs in each area transmit measurements in real-time over a local area network to the local PDC where Step 3) is carried out. These measurements (or a select subset of them) are sent to the ISO, where Steps 1) and 2) are carried out in parallel to Step 3) a). After Step 2) has been completed, the necessary information is transmitted back to the local areas so that they may complete Step 3) b) and c). We next describe each of these steps in detail.

IV. Steps for Real-Time Disturbance Localization

A. Step 1—Online Topology Identification

The first step is carried out by the ISO using real-time PMU measurements $y(t)$ in (7) streaming from each area. Here, we must assume that the p-area equivalent topology $\mathcal{G}^E$ exists,

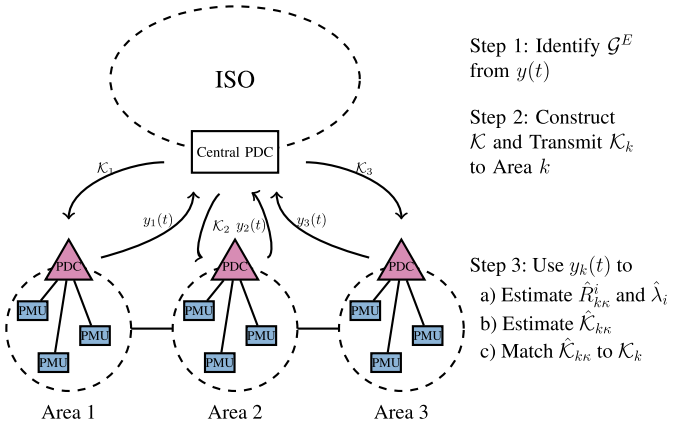

Fig. 1. Complete cyber-physical architecture for the real-time localization algorithm. Steps 1) and 2) are carried out by the central ISO, while Step 3) is carried out by the local areas independently.

and that the set of measured phase angles at the generator buses in $\mathcal{S}$ ensures that $\mathcal{G}^E$ is identifiable. Each coherent area can be represented by an equivalent generator, whose rotor angles and angular velocities are defined as $\delta^E = [\delta^E_1, \ldots, \delta^E_p]$ and $\omega^E \triangleq \dot{\delta}^E/\omega_s$. The linearized small-signal dynamics of the equivalent model can be written analogously to (4) as [15]

$$\begin{bmatrix} \Delta\dot{\delta}^E \\ \Delta\dot{\omega}^E \end{bmatrix} = \underbrace{\left[\begin{array}{c|c} 0_{p\times p} & \omega_s I_{p\times p} \\ \hline -L^E_m & -(M^E)^{-1}D^E \end{array}\right]}_{A^E} \begin{bmatrix} \Delta\delta^E \\ \Delta\omega^E \end{bmatrix} + \underbrace{\begin{bmatrix} 0 \\ (M^E)^{-1}e_l \end{bmatrix}}_{B^E} u(t) \quad (8)$$

where $M^E = \mathrm{diag}[m^E_1, \ldots, m^E_p]$ and $D^E = \mathrm{diag}[d^E_1, \ldots, d^E_p]$ are equivalent inertia and damping matrices, respectively, $u(t)$ is the same disturbance input as in (4), and $L^E_m \in \mathbb{R}^{p\times p}$ is the equivalent asymmetric Laplacian matrix with elements

$$\left[L^E_m\right]_{kj} = \begin{cases} -a^E_{kj}/m^E_k & \text{if } k \neq j \\ \sum_{\kappa\neq k} a^E_{k\kappa}/m^E_k & \text{if } k = j. \end{cases} \quad (9)$$

Notice that B^E in (8) now indicates that the input enters the lth area. The equivalent inertias m^E_k and damping factors d^E_k in (8) and the equivalent edge weights a^E_{kj} in (9) need to be estimated. We first assume that the equivalent topology $\mathcal{G}^E$ is a complete graph, meaning that every area is connected to every other area; then set a threshold $\alpha \in \mathbb{R}$ such that if $a^E_{kj} < \alpha$ then $a^E_{kj} = 0$, i.e., Areas k and j are not connected.

Because of the clustering and resulting time-scale separation of the states in (4), the phase angle of the ith machine (in Area k) can be written as

$$\Delta\delta_i(t) = \Delta\delta^E_k(t) + \Delta\delta^I_i(t) \quad (10)$$

for $i \in \mathcal{V}^k$, $k = 1, \ldots, p$, and where $\Delta\delta^I_i(t)$ denotes the fast component of $\Delta\delta_i(t)$ following from the fast eigenvalues of A in (4). The aggregate state $\Delta\delta^E_k(t)$ can be extracted from the measured values of $\Delta\delta_i(t)$, where $t = t_0, \ldots, t_f$, using modal decomposition techniques such as Prony's method [23] or the eigenvalue realization algorithm (ERA) [24]. Using $\Delta\delta^E(t)$, the ISO estimates the equivalent state matrix A^E defined in (8)

Algorithm 1 Online Topology Identification

Require: Measurements $y(t) = C\Delta\delta(t)$ for $t = t_0, \ldots, t_f$
1: Extract $\delta^E_k(t)$ for $k = 1, \ldots, p$
2: Estimate A^E from NLS problem (11)
3: Extract L^E_m from A^E

by formulating a nonlinear least-squares (NLS) problem

$$\min_{A^E} \int_{t_0}^{t_f} \left\| \Delta\delta^E(t) - \Delta\hat{\delta}^E(t, A^E) \right\|_2^2 dt \quad (11a)$$

$$\text{s.t.} \quad \Delta\hat{\delta}^E\left(t, A^E\right) = \hat{C}\exp\left(A^E(t - t_0)\right)\begin{bmatrix} \Delta\hat{\delta}^E(t_0) \\ \Delta\hat{\omega}^E(t_0) \end{bmatrix} \quad (11b)$$

where $\hat{C} = [I_{p\times p} \mid 0_{p\times p}]$. The NLS problem (11) can be solved in real-time using standard libraries such as MATLAB's optimization toolbox. Once A^E is estimated, the ISO extracts L^E_m from its bottom left $p \times p$ block shown in (8), and constructs the equivalent topology by inspecting the elements of L^E_m. The steps of this algorithm are summarized in Algorithm 1. Although the local operators persistently stream measurements to the central operator for monitoring purposes, Algorithm 1 is only initiated after a disturbance is detected. The algorithm exits once the aggregate equivalent model is found. The resulting L^E_m is the most up-to-date estimation of the equivalent topology, and therefore, will provide more accurate localization compared to the results in [15] where the equivalent topology was assumed to be fixed throughout.

B. Step 2—Constructing Localization Keys

For simplicity, we first assume that $u(t)$ is an impulsive function in the lth area (where l is unknown) and consider a single output of frequency—not phase angle—measurements from the kth equivalent generator (8). Note that the proceeding analysis will be easily generalized for outputs of generator phase angle measurements such as (7). In the case of frequency measurement, the input-output transfer function is

$$g^E_{kl}(s) \approx \sum_{i=1}^{p} \frac{R^i_{kl}}{s^2 + \lambda_i} \quad (12)$$

where λ_i is the ith eigenvalue of L^E_m. We use "$\approx$" in (12) because we have neglected any damping for simplicity.[1] The residue R^i_{kl} in (12) can be written as the product of the mode controllability factor and mode observability factor [26] as

$$R^i_{kl} = \underbrace{[v_i]_l}_{\text{obsv. factor}} \underbrace{\left[w_i^T M^{-1}\right]_k}_{\text{ctrl. factor}} \quad (13)$$

where v_i and w_i are the right and left eigenvectors corresponding to λ_i of L^E_m. Hence, the sign of R^i_{kl} is determined by the relative nodal domain locations of k and l. For example, if $\mathcal{D}_1$ and $\mathcal{D}_2$ are adjacent λ_i nodal domains (Definition 2), then

$$\mathrm{sign}(R^i_{kl}) = \begin{cases} + & \text{if } k, l \in \mathcal{D}_1 \setminus \mathcal{D}_2 \\ - & \text{if } k \in \mathcal{D}_1 \setminus \mathcal{D}_2 \text{ and } l \in \mathcal{D}_2 \setminus \mathcal{D}_1 \\ 0 & \text{if } k \in \mathcal{D}_1 \cap \mathcal{D}_2 \text{ or } l \in \mathcal{D}_1 \cap \mathcal{D}_2. \end{cases}$$

[1] In practice it is not necessary to neglect the damping factors. We refer the reader to [25] for details.

Algorithm 2 Centralized Localization Key Building

Require: Equivalent Laplacian L_m^E

1: Compute eigenvalues and eigenvectors of L_m^E
2: **for** $k = 1 \rightarrow p$ **do**
3: Construct row of localization keys $\mathcal{K}_k$

$$[\mathcal{K}_k]_l = \{\text{sign}([v_2]_l[w_2]_k), \ldots, \text{sign}([v_p]_l[w_p]_k)\}$$

▷ Only require $l > k$ since keys are symmetric
4: **end for**
5: Broadcast localization keys to Area Operators

It is straightforward to generalize this example to all of the λ_i nodal domains (not only adjacent nodal domains). Thus, using L_m^E identified in Algorithm 1, we can build a mapping between the relative input-output locations and the transfer function residues (13). We refer to this mapping as a localization key, and define it formally as

$$\mathcal{K}_{kl} = \{\text{sign}([v_2]_l[w_2]_k), \ldots, \text{sign}([v_p]_l[w_p]_k)\}. \quad (14)$$

We also define an array of these localization keys as $\mathcal{K} = [\mathcal{K}_{kl}]$, which provides a mapping of all input-output locations (at the area level). In other words, the kth row (column) of $\mathcal{K}$, denoted by $\mathcal{K}_k$, is associated with Area k. This row (column) consists of the keys that relate an input in any (other) area to an output taken from Area k. Furthermore, if we consider every input-output pair, we may define a matrix of residues corresponding to each eigenvalue as

$$R^i = \left[R_{kl}^i\right] = v_i w_i^T M^{-1} \quad (15)$$

for $i = 1, \ldots, p$. The matrix R^i in (15) is symmetric, and the λ_i nodal domains of v_i and w_i are identical, which implies that the array of localization keys $\mathcal{K}$ is symmetric [15].

Algorithm 2 outlines the steps which the central operator must take in order to construct $\mathcal{K}$ in real-time. The algorithm starts immediately after Algorithm 1 exits, and the most complex step occurs in line 1, which involves an eigenvalue decomposition of the $p \times p$ matrix L_m^E. Starting on line 3, the individual keys $\mathcal{K}_{kl}$ are constructed according to (14). Notice that the array of keys is symmetric and the diagonal entries are trivial, i.e., $\mathcal{K}_{kk} = \{+, \ldots, +\}$. Hence, only the upper triangle of the array needs to be computed. Finally, the central operator transmits the row of keys $\mathcal{K}_k$ to the respective local area. In Section V, we illustrate the construction of an array of localization keys for a four-area equivalent partitioning of the IEEE 39-bus system.

Clearly, the real component of the residues R_{kl}^i in (12)—the transfer function from $u(t)$ to $\Delta\omega^E(t)$—contains information relating the location of the input relative to the location of the output through the λ_i nodal domains (Definition 1). In [15], it is shown that the residues of the transfer function from $u(t)$ in (8) to $y(t)$ in (7) contain identical information. In this case, however, that information is stored in the imaginary part of the transfer function residues. It follows that the operator in the kth area can easily use his measurements $y_k(t)$ to estimate the transfer function (12) and hence the residues in (13), then exploit the information they carry. We describe this algorithm next.

C. Step 3—Real-Time Input Localization

Step 3 is carried out entirely by the local area operators individually, i.e., each operator uses his own and only his own measurements, and is initialized as soon as the disturbance has been detected. The goal of this step is to exploit the locational information carried by the transfer function residues (recall the discussion from the previous section). This can be understood in three distinct parts: estimate the system slow poles and residues of (12), build an estimated localization key $\hat{\mathcal{K}}_{\kappa k}$, then compare the estimated key to the set provided by the central operator. Algorithm 3 summarizes Step 3 and its three parts are forthwith described in detail.

1) Estimate Slow Poles and Residues: The operator in Area k must estimate the equivalent transfer function (12), in particular, he must determine its poles and residues. It is important to emphasize that this part of Step 3—lines 1 and 2 in Algorithm 3—can be carried out in parallel to Step 1, i.e., starting at $t = t_f$, which is being executed by the central ISO. Since we have assumed $\mathcal{G}^E$ is connected, the operator in Area k can use his measurements $y_k(t) = C_k\Delta\delta(t)$ from a set of generator buses $\mathcal{S}^k \subseteq \mathcal{V}^k$ to find the poles and residues of interest. This is done by running a standard system identification algorithm to construct the transfer function from $u(t)$ in (4) to $y_k(t)$, then truncating this transfer function to only consider the slow poles and residues. The result of this subroutine is the estimated values of the system poles and residues, which we denote by $\hat{\lambda}_i$ and $\hat{R}_{\kappa k}^i$, for $i = 1, \ldots, \hat{p}$, respectively. Notice that since the input location is unknown we have used the dummy variable κ. Also notice that depending on the type of disturbance, e.g., transient, harmonic, etc., and due to other un-modeled dynamics in the power system, the system identification algorithm may identify more than $p - 1$ slow oscillatory components. Hence, we use $\hat{p}$ to denote the total number of slow modes (including any dc modes) recovered by the system identification.

2) Build Estimated Localization Key $\hat{\mathcal{K}}_{\kappa k}$: Before proceeding further, the local operator requires the modes of A^E and localization keys $\mathcal{K}_k$. The slow oscillatory components closest to the natural modes of A^E and their corresponding residues are used to build an estimated localization key $\hat{\mathcal{K}}_{\kappa k}$ according to (13) and (14). In the case that additional slow modes are identified, the residues used in $\hat{\mathcal{K}}_{\kappa k}$ may need to be corrected. Due to space limitations we refer the reader to [25] for details regarding why and how to correct the signs of these residues.

3) Compare Estimated Key: Recall that the signs of the transfer function residues contain information about the relative input-output nodal domain locations, and that the estimated $\hat{\mathcal{K}}_{\kappa k}$ is a mapping between the residues and these locations. Since the output location k is known, the localization problem can be solved by determining κ. This is done by comparing $\hat{\mathcal{K}}_{\kappa k}$ to the most up-to-date set of keys $\mathcal{K}_k$ provided by the central ISO. Matching key(s) indicate possible area(s) in which the disturbance input may have entered. For example,

Algorithm 3 Real-Time Attack Localization From Area k

Require: Local PMU measurements, localization keys $\mathcal{K}_k$, modes of A^E

1: Run System Identification to estimate $(\hat{A}^E, \hat{B}^E, \hat{C}^E)$
2: Extract slow modes $\hat{\lambda}_i$ $i = 2, \ldots, \hat{p}$, and residues $\hat{R}^i_{\kappa k}$, $i = 2, \ldots, \hat{p}$
3: Wait to receive $\mathcal{K}_k$ and modes of L^E_m from central operator
4: Construct estimated localization key

$$\hat{\mathcal{K}}_{\kappa k} = \{\text{sign}(\hat{R}^2_{\kappa k}), \ldots, \text{sign}(\hat{R}^p_{\kappa k})\}$$

5: **for** $\kappa = 1 \rightarrow p$ **do**
6: Compare $\hat{\mathcal{K}}_{\kappa k}$to elements of $\mathcal{K}_k$
7: **if** Match, i.e., $\hat{\mathcal{K}}_{\kappa k} = [\mathcal{K}_k]_l$ **then**
8: Attack may have occurred in Area l
9: **end if**
10: **end for**

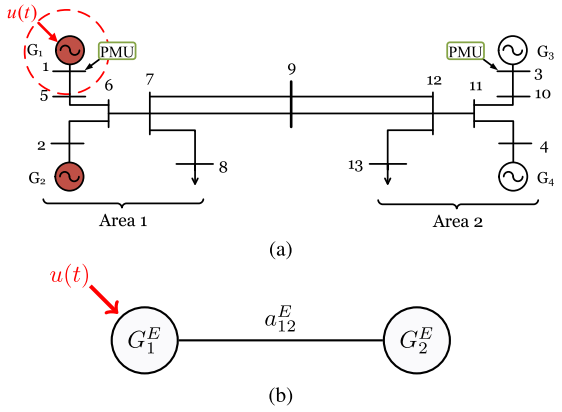

Fig. 2. (a) Kundur system with areas: $G^E_1 = \{G_1,\ G_2\}$ and $G^E_2 = \{G_3,\ G_4\}$. (b) Equivalent aggregate topology $\mathcal{G}^E$.

if $\hat{\mathcal{K}}_{\kappa k} = [\mathcal{K}_k]_3$, then the disturbance may have occurred in Area 3. Notice that this matching does not have to be unique. In fact, it should be clear that this matching will only be unique if and only if for $k \neq l$ we have $[\mathcal{K}_i]_k \neq [\mathcal{K}_i]_l\ \forall i = 1, \ldots, p$. For example, if the equivalent network is a complete graph, then the set of keys $\mathcal{K}_k$ constructed in Step 2 will preclude uniquely identifying the area in which the disturbance entered. We refer the reader to [15] for further discussion of classes of graphs in which this step will result in a unique localization. The next section provides a concrete implementation of Steps 1)–3) using realistic power system models.

V. Case-Studies

These case studies provide a concrete implementation of Steps 1)–3). We begin by describing the steps on a four-machine two-area Kundur system (Fig. 2) following an excitation of generator 2. Afterwards, the localization algorithm is demonstrated on a modified IEEE 39-bus model (Fig. 4).

A. Two-Area Kundur System

The system consists of four generators G_1–G_4 as shown in Fig. 2. The system parameters are provided in `d2asbegh.m` in the Power System Toolbox [27]. Generators G_1 and G_2 belong to Area 1, while G_3 and G_4 belong to Area 2. At $t_0 = 0$ an attack is induced by suddenly changing the voltage reference of the excitation controller of G_1 (inside of Area 1), causing a disturbance in the network. The phase angle and frequency of G_1 and G_3 are measured until $t_f = 10$ sec using PMUs at their terminal buses. Fig. 3 shows these output measurements that are sent to the central operator. Thereafter, Steps 1)–3) are carried out as follows.

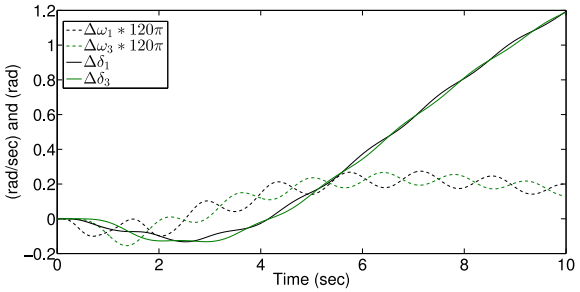

Fig. 3. Measured outputs following an attack in the two-area Kundur system.

TABLE I
Input Localization Keys for the Kundur System in Fig. 2

Area	1	2
1	{+}	{−}
2	{−}	{+}

1) Topology Identification: At $t = t_f$, the central operator takes the measurements $y(t)$ shown in Fig. 3 and initializes Algorithm 1. Next, the NLS problem (11) is formulated and solved in t_1 s. The identified equivalent topology $\mathcal{G}^E$ for the two-area system is shown in Fig. 3(b), and the asymmetric Laplacian matrix is

$$L^E_m = \begin{bmatrix} -10.97 & 10.97 \\ 8.56 & -8.59 \end{bmatrix}. \tag{16}$$

The nonzero eigenvalues of A^E are

$$\{-0.052 \pm 4.4065j\}. \tag{17}$$

2) Centralized Key-Building: At this point $(t = t_f + t_1)$, the central operator runs Algorithm 2 to determine the array of localization keys. He first runs an eigenvalue decomposition on L^E_m in (16) to determine the λ_2 nodal domains. There are always exactly two nodal domains corresponding to λ_2—one positive and one negative—hence one of the aggregate areas comprises the positive nodal domain while the other comprises the negative nodal domain. The central operator next constructs the 2×2 array of localization keys $\mathcal{K}$. For the two-area system, the length of each key is $(2 - 1) = 1$ bit. The localization keys are shown in Table I. This entire step takes t_2 s. The central operator transmits individual rows of Table I to the local area operator corresponding to that row. That is, the first row is sent to Area 1 and the second row is sent to Area 2. Assuming there is some network delay t_d, the row of keys $\mathcal{K}_k$ is received at the control room of Area k at time $t = t_f + t_1 + t_2 + t_d$.

TABLE II
SLOW POLES AND RESIDUES RECOVERED FROM $\Delta\delta_3$

Pole	Residue
$-0.0618 \pm 4.4053j$	$0.0058 \pm 0.0015j$

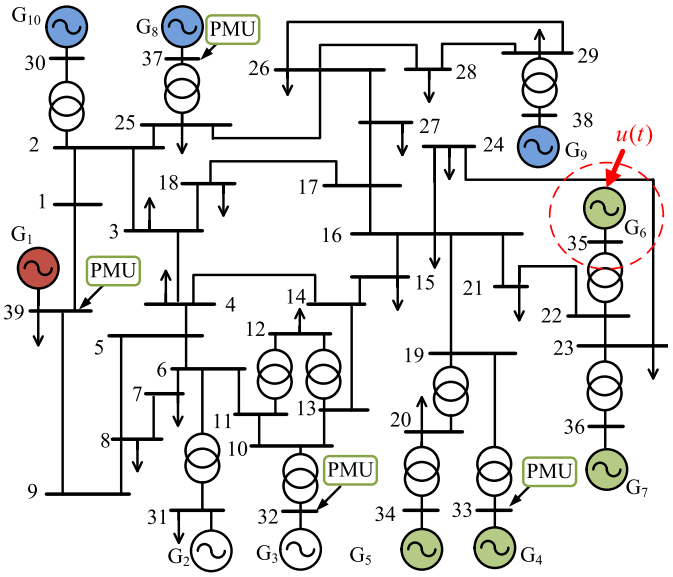

Fig. 4. IEEE 39-bus power system model with areas: $G_1^E = \{G_1\}$, $G_2^E = \{G_2,\ G_3\}$, $G_3^E = \{G_4,\ G_5,\ G_6,\ G_7\}$, and $G_4^E = \{G_8,\ G_9,\ G_{10}\}$.

3) Attack Localization: The local area operators can begin Step 3 at the same time as the central operator initializes Step 1). For example, let us consider the perspective of the operator in Area 2. Using his measurements $\Delta\delta_3(t)$, $t = t_0, \ldots, t_f$, from generator G_3, he starts Algorithm 3. The estimated poles and residues are shown in Table II. If this subroutine takes $t_3 < t_1 + t_2 + t_d$ s to execute, the operator in Area 2 must wait until he receives $\mathcal{K}_2$ and the estimates of the slow poles from the central ISO at $t = t_f + t_2 + t_d$ before proceeding.

Once the set of keys $\mathcal{K}_2$ and slow poles (17) have been received, the operator uses only the poles in Table II that match those in (17). The corresponding residues are then used to construct $\hat{\mathcal{K}}_{\kappa 2} = \{-\}$. This estimated key is compared to those in $\mathcal{K}_2$ (the second row of Table I). In this case, the estimated key only matches the first element of $\mathcal{K}_2$. Hence, the operator in Area 2 infers that the disturbance must have occurred in Area 1. An identical procedure can be carried out by the operator in Area 1 with the same conclusion.

B. IEEE 39-Bus System

We next summarize the results of the localization algorithm following an attack on generator G_6 in Area 3 in a modified IEEE 39-bus model[2] shown in Fig. 4. The model parameters of Fig. 4 have been derived from [28]. We consider a 4-area partitioning of the network. The attack occurs at $t_0 = 0$, and by $t_f = 20$ sec enough data has been recorded to capture the slow oscillatory modes of the network. Fig. 5 shows the output measurements that are sent to the central operator. Steps 1)–3) are carried out as follows. The identified equivalent topology $\mathcal{G}^E$ is shown in Fig. 6(a), with asymmetric Laplacian matrix

$$L_m^E = \begin{bmatrix} -8.883 & 5.497 & 0 & 3.386 \\ 12.828 & -33.159 & 16.981 & 3.350 \\ 0 & 8.612 & -11.174 & 2.562 \\ 10.392 & 4.406 & 6.645 & -21.443 \end{bmatrix}. \quad (18)$$

Notice that in Fig. 6(a), Areas 1 and 3 are not connected and the corresponding elements in the identified Laplacian matrix (18) are identically zero. The eigenvalues of A^E are

$$\{-0.30 \pm 3.083j,\ -0.27 \pm 4.966j,\ -0.28 \pm 6.297j\}. \quad (19)$$

The resulting nodal domains corresponding to λ_k, $k = 2, \ldots, 4$, are shown in Fig. 6. The array of localization keys $\mathcal{K}$ constructed using these nodal domains is provided in Table III.

Using his measurements of phase angle $y_1(t)$, $t = t_0, \ldots, t_f$, from generator 1, the local operator starts Algorithm 3. The estimated poles and residues are shown in Table IV. Notice that two additional slow poles were identified by ERA. Once the set of keys $\mathcal{K}_1$ and slow poles (19) have been received, the local operator uses the estimated poles in Table IV that match those sent by the central ISO (shown in bold) and the corresponding residues to construct $\hat{\mathcal{K}}_{\kappa 1}$. Evaluating the sign of the real part of the residues in Table IV according to (14), he finds $\hat{\mathcal{K}}_{\kappa 1} = \{-, +, +\}$, which matches the third element of $\mathcal{K}_1$ in Table III, i.e., $\hat{\mathcal{K}}_{\kappa 1} = [\mathcal{K}_1]_3$.

[2]The lines typically connecting buses 4 and 5 and buses 16 and 17 has been removed to improve the coherency of the areas.

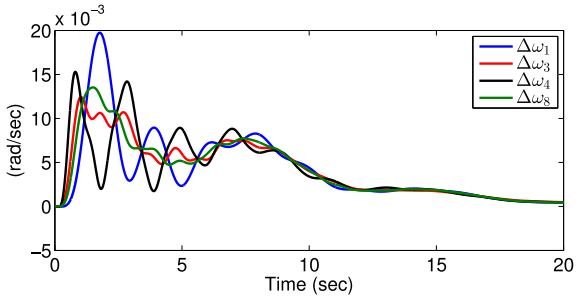

Fig. 5. Measured outputs following an attack in IEEE 39-bus system.

TABLE III
INPUT LOCALIZATION KEYS FOR THE IEEE 39-BUS SYSTEM IN FIG. 4

Area	1	2	3	4
1	·	$\{-,+,-\}$	$\{-,+,+\}$	$\{+,-,+\}$
2	·	·	$\{+,+,-\}$	$\{-,-,-\}$
3	·	·	·	$\{-,-,+\}$
4	·	·	·	·

TABLE IV
POLES AND RESIDUES RECOVERED FROM $\Delta\omega_1$. VALUES THAT ARE USED TO BUILD THE LOCALIZATION KEY ARE IN BOLDFACE

Pole	Residue
$-0.2234 \pm 0.8993j$	$0.2823 \pm 0.5200j$
$-0.3165 \pm 2.0205j$	$-0.0205 \pm 0.4301j$
$\mathbf{-0.3614 \pm 3.1108j}$	$\mathbf{0.0607 \pm 0.2441j}$
$\mathbf{-0.3196 \pm 5.0041j}$	$\mathbf{-0.0352 \pm 0.1505j}$
$\mathbf{-0.3479 \pm 6.2280j}$	$\mathbf{0.1185 \pm 0.0560j}$

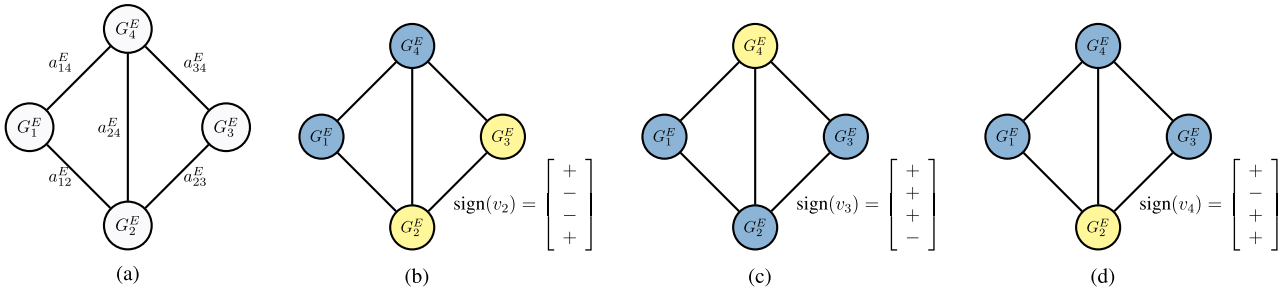

Fig. 6. (a) Identified $\mathcal{G}^E$ for IEEE 39-bus model. (b)–(d) λ_2–λ_4 nodal domains of $\mathcal{G}^E$. Notice that there are only two nodal domains for each of λ_2–λ_4.

The operator in Area 1, therefore, infers that the disturbance has occurred in Area 3. This procedure can be repeated by the operators in Areas 2, 3, and 4 separately.

VI. Conclusion

In this paper, we developed a novel measurement-based disturbance localization algorithm for large-scale power systems that can be carried out in real-time using synchrophasor measurements. The cyber-physical infrastructure underlying the modern power grid enables the three steps of the proposed algorithm to be completely measurement-based, that is relying on minimal information of the actual power system network. Therefore, it captures the most up-to-date wide-area network configuration without relying on a static model of the network as is used in conventional monitoring. The algorithm makes use of concepts from graph theory, and yet is numerically efficient to execute. It also preserves data privacy of the different utilities. The different steps of the algorithm were validated using IEEE 9-bus and 39-bus power system models.

References

[1] A. Phadke and J. Thorp, *Synchronized Phasor Measurements and Their Applications* (Power Electronics and Power Systems). New York, NY, USA: Springer, 2008.

[2] J. Quintero, G. Liu, and V. Venkatasubramanian, "An oscillation monitoring system for real-time detection of small-signal instability in large electric power systems," in *Proc. IEEE Power Eng. Soc. Gen. Meeting*, Tampa, FL, USA, Jun. 2007, pp. 1–8.

[3] L. Zhao and A. Abur, "Multi area state estimation using synchronized phasor measurements," *IEEE Trans. Power Syst.*, vol. 20, no. 2, pp. 611–617, May 2005.

[4] S. Ghiocel *et al.*, "Phasor-measurement-based state estimation for synchrophasor data quality improvement and power transfer interface monitoring," *IEEE Trans. Power Syst.*, vol. 29, no. 2, pp. 881–888, Mar. 2014.

[5] A. Chakrabortty, "Wide-area damping control of power systems using dynamic clustering and TCSC-based redesigns," *IEEE Trans. Smart Grid*, vol. 3, no. 3, pp. 1503–1514, Sep. 2012.

[6] Y. Liu, P. Ning, and M. K. Reiter, "False data injection attacks against state estimation in electric power grids," *ACM Trans. Inf. Syst. Sec.*, vol. 14, no. 13, pp. 1–33, Jun. 2011.

[7] O. Kosut, L. Jia, R. J. Thomas, and L. Tong, "Malicious data attacks on the smart grid," *IEEE Trans. Smart Grid*, vol. 2, no. 4, pp. 645–658, Dec. 2011.

[8] A. Giani *et al.*, "Smart grid data integrity attacks: Characterizations and countermeasures," in *Proc. IEEE Int. Conf. Smart Grid Commun. (SmartGridComm)*, Brussels, Belgium, Oct. 2011, pp. 232–237.

[9] A. Teixeira, S. Amin, H. Sandberg, K. Johansson, and S. Sastry, "Cyber security analysis of state estimators in electric power systems," in *Proc. 49th IEEE Conf. Decis. Control*, Atlanta, GA, USA, Dec. 2010, pp. 5991–5998.

[10] O. Vukovic, K. C. Sou, G. Dan, and H. Sandberg, "Network-aware mitigation of data integrity attacks on power system state estimation," *IEEE J. Sel. Areas Commun.*, vol. 30, no. 6, pp. 1108–1118, Jul. 2012.

[11] F. Pasqualetti, F. Dorfler, and F. Bullo, "Attack detection and identification in cyber-physical systems," *IEEE Trans. Autom. Control*, vol. 58, no. 11, pp. 2715–2729, Nov. 2013.

[12] R. B. Myers and D. J. Trudnowski, "Effects of forced oscillations on spectral-based mode-shape estimation," in *Proc. IEEE Power Eng. Soc. Gen. Meeting*, Vancouver, BC, Canada, Jun. 2013, pp. 1–6.

[13] W. Wang and Z. Lu, "Cyber security in the smart grid: Survey and challenges," *Comput. Netw.*, vol. 57, no. 5, pp. 1344–1371, 2013.

[14] Z. Zhang, S. Gong, A. D. Dimitrovski, and H. Li, "Time synchronization attack in smart grid: Impact and analysis," *IEEE Trans. Smart Grid*, vol. 4, no. 1, pp. 87–98, Mar. 2013.

[15] T. R. Nudell and A. Chakrabortty, "Graph-theoretic methods for measurement-based input localization in large networked dynamic systems," *IEEE Trans. Autom. Control*, 2015, Doi: 10.1109/TAC.2015.2398911.

[16] S. Nabavi and A. Chakrabortty, "Topology identification for dynamic equivalent models of large power system networks," in *Proc. Amer. Control Conf.*, Washington, DC, USA, Jun. 2013, pp. 1138–1143.

[17] J. Ma, R. Diao, Y. Makarov, P. Etingov, and J. Dagle, "Event classification and identification based on characteristic ellipsoid of phasor measurement," in *Proc. North Amer. Power Symp. (NAPS)*, Boston, MA, USA, Aug. 2011, pp. 1–6.

[18] M.-A. Massoumnia, G. C. Verghese, and A. Willsky, "Failure detection and identification," *IEEE Trans. Autom. Control*, vol. 34, no. 3, pp. 316–321, Mar. 1989.

[19] T. Biyikoğlu, J. Leydold, and P. F. Stadler, *Laplacian Eigenvectors of Graphs*, J. Morel, F. Takens, and G. Teissier, Eds. Berlin, Germany: Springer-Verlag, 2007.

[20] P. M. Anderson and A. A. Fouad, *Power System Control and Stability*, 2nd ed. Hoboken, NJ, USA: Wiley, 2003.

[21] F. Dorfler and F. Bullo, "Kron reduction of graphs with applications to electrical networks," *IEEE Trans. Circuits Syst. I, Reg. Papers*, vol. 60, no. 1, pp. 150–163, Jan. 2013.

[22] J. Chow and P. Kokotovic, "Time scale modeling of sparse dynamic networks," *IEEE Trans. Autom. Control*, vol. 30, no. 8, pp. 714–722, Aug. 1985.

[23] J. Hauer, C. Demeure, and L. Scharf, "Initial results in Prony analysis of power system response signals," *IEEE Trans. Power Syst.*, vol. 5, no. 1, pp. 80–89, Feb. 1990.

[24] J.-N. Juang and R. Pappa, "An eigensystem realization algorithm for modal parameter identification and model reduction," *J. Guid. Control Dynam.*, vol. 8, no. 5, pp. 620–627, 1985.

[25] T. R. Nudell and A. Chakrabortty, "A graph-theoretic algorithm for localization of forced harmonic oscillation inputs in power system networks," in *Proc. Amer. Control Conf.*, Portland, OR, USA, Jun. 2014, pp. 1334–1340.

[26] N. Martins and L. Lima, "Determination of suitable locations for power system stabilizers and static VAR compensators for damping electromechanical oscillations in large scale power systems," in *Proc. Power Ind. Comput. Appl. Conf.*, Seattle, WA, USA, May 1989, pp. 74–82.

[27] J. Chow and K. Cheung, "A toolbox for power system dynamics and control engineering education and research," *IEEE Trans. Power Syst.*, vol. 7, no. 4, pp. 1559–1564, Nov. 1992.

[28] T. Athay, R. Podmore, and S. Virmani, "A practical method for the direct analysis of transient stability," *IEEE Trans. Power App. Syst.*, vol. 98, no. 2, pp. 573–584, Mar. 1979.

Thomas R. Nudell (S'10) received the B.A. degree in physics from Kalamazoo College, Kalamazoo, MI, USA, in 2009, and the M.S. degree in electrical engineering along with a graduate certificate in renewable electric energy systems and the Ph.D. degree in electrical engineering from North Carolina State University, Raleigh, NC, USA, in 2011 and 2014, respectively.

His current research interests include monitoring, analysis, and control of large-scale networked dynamic systems, and power systems.

Dr. Nudell is a Member of Phi Beta Kappa.

Seyedbehzad Nabavi (S'12) received the B.S. degree from the Amirkabir University of Technology (Tehran Polytechnic), Tehran, Iran, in 2009, and the M.S. degree from North Carolina State University, Raleigh, NC, USA, in 2011, where he is currently pursuing the Ph.D. degree, all in electrical engineering.

His current research interests include applied control theory and wide-area monitoring of large-scale power systems.

Aranya Chakrabortty (S'02–M'06–SM'15) received the Ph.D. degree in electrical engineering from Rensselaer Polytechnic Institute, Troy, NY, USA, in 2008.

Since 2010, he has been an Assistant Professor in the Department of Electrical and Computer Engineering, North Carolina State University, Raleigh, NC, USA, where he is also affiliated with the FREEDM Systems Center. His current research interests include all branches of control theory with applications to power systems, especially in wide-area monitoring and control using synchrophasors.

Dr. Chakrabortty was the recipient of the National Science Foundation CAREER Award in 2011.